TITLE:

Strain Variations of the Yamasaki Fault Zone, Southwest Japan, Derived from Extensometer Observations. Part 2 --On the Short-term Strain Variations Derived from Strain Steps--

AUTHOR(S):

WATANABE, Kunihiko

CITATION:

WATANABE, Kunihiko. Strain Variations of the Yamasaki Fault Zone, Southwest Japan, Derived from Extensometer Observations. Part 2 --On the Short-term Strain Variations Derived from Strain Steps--. Bulletin of the Disaster Prevention Research Institute 1991, 41(2): 53-85

ISSUE DATE:

1991-06

URL:

http://hdl.handle.net/2433/124978

RIGHT:

京都大学学術情報リポジトリ
KURENAI 紅
Kyoto University Research Information Repository

Bull. Disas. Prev. Res. Inst., Kyoto Univ., Vol. 41, Part 2, No. 355, June, 1991

Strain Variations of the Yamasaki Fault Zone, Southwest Japan, Derived from Extensometer Observations

Part 2 — On the Short-term Strain Variations Derived from Strain Steps —

By Kunihiko WATANABE

(Manuscript received on March 6, 1991)

Abstract

Coseismic strain steps during the Yamasaki fault earthquake sequence and some other distant large earthquakes have been observed with the extensometers at the Yasutomi Observation Vault of the Yamasaki Fault Observation Station. Usually, the amplitudes of those strain steps are larger than those theoretically expected and the polarities of strain steps also disagree with theoretically expected ones. The directions of the principal strain axis of each strain released by strain steps were frequently normal or parallel to the fault strike. Therefore, the pattern of the strain release strongly depends on the neighboring structure, namely, existence of the fault. In order to confirm this mechanism, a mechanical model for numerical simulations is presented. The results of these simulations could explain reasonably well the characteristics of the observed strain steps. The rather large amount of strain released by strain steps is considered to be the strain which has been previously accumulated in and around the observation site and is released by seismic waves. In the case of the Yasutomi Observation Vault, this kind of strain accumulation is originated by thermal deformation of the basement rock caused by surface temperature variations.

1. Introduction

Sudden changes in strain variations, "strain steps", are occasionally detected on the continuous records of extensometer observations. From observational experiences, a few of these strain changes are consistent with those theoretically expected by assuming that the strain variations at the hypocenter is propagated elastically or viscoelastically to the observation site. However, most of the observed strain changes cannot be explained theoretically. Furthermore, some of those sudden changes remain as permanent discontinuities in strain, while others return to their original levels gradually.

There have been a number of theoretical investigations on strain steps directly related to earthquake origin. For example, Press (1965)[1] obtained displacements and strains on the ground surface caused by distant earthquakes. Sato and Matsu'ura (1974)[2] and Matsu'ura and Sato (1975)[3] calculated displacements and strains propagated through an elastic medium. Matsu'ura et al. (1981)[4] also calculated those in layered media with a viscoelastic layer.

On the other hand, there are some observational investigations on strain steps. For example, Wideman and Major (1967)[5] obtained an empirical formula, $M=1.1+1.74\ log(D)$,

expressing a relation between the earthquake magnitude(M) and epicentral distance(D) for strain steps down to 10^{-9}. Takemoto and Takada(1969)[6] also obtained a formula, $M=0.4+2.2\ log(D)$, down to 10^{-8} strain steps.

Strain steps are occasionally observed with the extensometers at the Yasutomi Observation Vault of the Yamasaki Fault Observation Station. The observed strain steps are not always explained by such theoretical or empirical results as the above mentioned, which implies that these strain steps strongly reflect the physical conditions of the observation site.

In this study, we will investigate the strain steps observed at the Yasutomi Observation Vault and try to clarify the short-term behavior of the fault zone. The strain steps caused by the Yamasaki fault earthquake sequence in 1984 and those caused by distant earthquakes are analyzed. A mechanical model which represents the characteristic strain steps in a fault zone will also be presented.

2. The Yasutomi fault and its observation system

The Yasutomi fault and its extensometer observation system are explained briefly. Details are described by Oike et al. (1981)[7], Watanabe et al. (1983)[8] and the author in part 1 of the present paper[9]. The structure of the Yasutomi fault has two distinguishable zones, "the fault zone" and "the fractured zone". In this article, "the fault zone" is defined as a belt zone of 100–200 meters thickness. Inside the fault zone, there are some "fractured zones" which are thin zones of fractured rock and fault clay. In the case of the Yasutomi fault, these fractured zones are almost parallel to the fault zone.

Electromagnetic Research Group for the Active Fault (1982)[10] revealed the existence of the relatively low resistivity of 1000 ohm • m in the belt zone of two kilometers width along the Yasutomi fault. Inside this belt zone, they found a further low resistivity zone of 100–400 ohm • m, 100–200 meters width, which seems to correspond to "the fault zone" mentioned above. Furthermore, very low resistivity streaks of 20 ohm • m with a few tens of meters thickness are recognized. These extremely low resistivity may be caused by the existence of "the fractured zones". The observation vault is wholly included in "the fault zone" and lies across "the fractured zones". By considering these structural stratum, characteristic behaviors of both the fault and fractured zones have been investigated, with regard to long-term strain variations, earth tides, surface waves and S-waves[9,11~13]. Detailed investigation of the behavior of the fractured zones inside the fault zone will play an important role for better understanding of the physical behavior of a fault system in the crust.

The topography around the Yamasaki Fault Observation Station and the location of the Yasutomi Observation Vault are illustrated in **Fig. 1.** Spatial relation between the Yasutomi Observation Vault and the Chugoku Expressway[14] and the arrangement of extensometer sensors are shown in **Fig. 2.** As described in part 1[9], we call the strain between the fixed-end of the extensometer rods and i-th sensor "fixed-end strain" of component 0–i. By taking the difference between the i-th and j-th sensors, we can calculate the strain between these two sensors. We call this kind of strain "partial

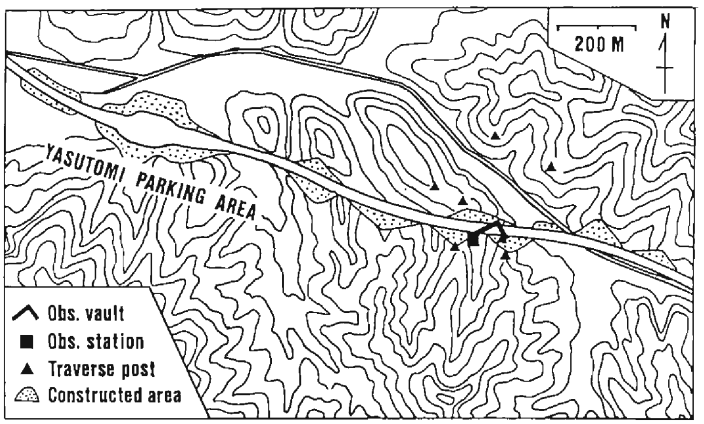

Fig. 1. Topography around the Yamasaki Fault Observation Station (■). The Yasutomi Observation Vault (L-shaped) is situated just under the Chugoku Expressway. Solid triangles are the traverse posts of the Yasutomi–Usuzuku Baseline Network for geodetic measurements.

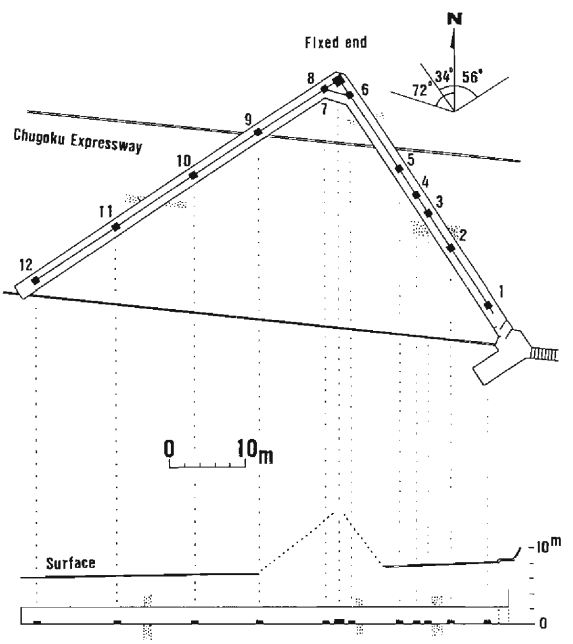

Fig. 2. Spatial relation between the observation vault and the Chugoku Expressway. Numerals denote the displacement sensors of the extensometers. Some fractured zones are illustrated by shadows. The lower figure shows the vertical section of the vault and the expressway. The corner of the vault is located under the northern mountainous area.

Table 1. Distanoes between the fixed-end and each displacement sensor and directions of the extensometer rods at the Yasutomi Observation Vault

sensor No.	distance from the fixed end	direction of the rod
1	35.78[m]	N34°W
2	26.86	〃
3	21.49	〃
4	18.60	〃
5	14.55	〃
6	3.02	〃
7	3.82	N72°W
8	2.40	N56° E
9	12.76	〃
10	22.76	〃
11	34.83	〃
12	47.89	〃

strain" of component i–j. The directions of the extensometer rods and the distances between the fixed–end and each displacement sensor are listed in **Table 1.**

Differential transformers are used as the displacement sensors of the extensometers at the Yasutomi Observation Vault. The extensometer rods are hung by stainless strings 0.1 millimeter in diameter. As the Yasutomi Observation Vault is just below the Chugoku Expressway, traffic vibrations with amplitudes of about 10^{-3} cm/sec and dominant frequencies of 10 Hz or more are always fed to the extensometer system. Therefore, no frictional disturbance is accumulated at any portion of the instruments. Furthermore, the state of the extensometers is sometimes checked by a test in which external force is applied to the ends of rods and removed. The hysteresis of the instruments and the sensitivity of the extensometers are examined by this test. The observed data are then confirmed to show natural phenomena without any instrumental disturbances.

In order to reduce traffic noise from the expressway, the output signals of the extensometers of periods shorter than one minute are cut off by active filters. These filtered signals are sampled by a multiplexer at one-minute intervals, and sent to the Disaster Prevention Research Institute of Kyoto University in Uji by a telephone line. The transmitted data are received and stored by a mini-computer system every minute. Through this data acquiring process, the time accuracy of extensometer data is within two minutes.

Because of the limited memory capacity of our observing system, minute data are stored on the CPU system for only 10 days or less. Important data are saved by a CMT recorder. Plotting recorders are also used for monitoring. These two kinds of data are used for the strain step analysis in this study.

3. Strain steps caused by the Yamasaki fault earthquake sequence

3. 1 Outline of the Yamasaki fault earthquake sequence

A moderate-size earthquake of M5.6 occurred at 09h39m on May 30th, 1984. We refer to this earthquake as "the Yamasaki fault earthquake" in this article. Nishigami (1984)[15] determined the hypocenters of this earthquake and aftershock sequence with good accuracy. The hypocenter of the main shock(M5.6) is located on the Kuresaka-toge fault which is a fault segment belonging to the Yamasaki fault system. The direction of the main shock from the Yasutomi Observation Vault is N155°W and the epicentral and hypocentral distances are 3.3 and 21.0 kilometers, respectively. The fault plane solution of the main shock derived by Nishida(1985)[16] indicates a left-lateral strike slip type, and that the strike of one of the nodal planes almost coincides with the strike of the Kuresaka-toge fault. The hypocentral distributions determined by Nishigami

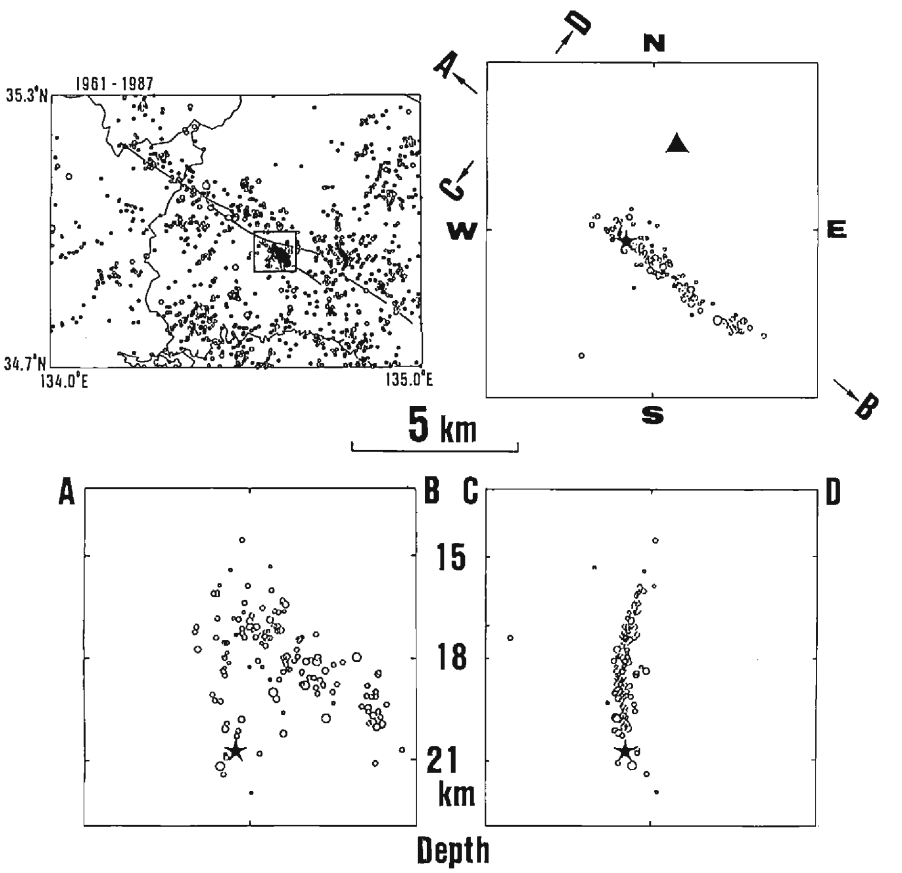

Fig. 3. Hypocentral distributions of the Yamasaki fault earthquake sequence determined by Nishigami (1984)[15]. Epicentral distributions of M≧1.6 on the left-upper of the figure are obtained by the Tottori Microearthquake Observatory[17]. Solid lines from NW to SE denote the Yamasaki fault system.

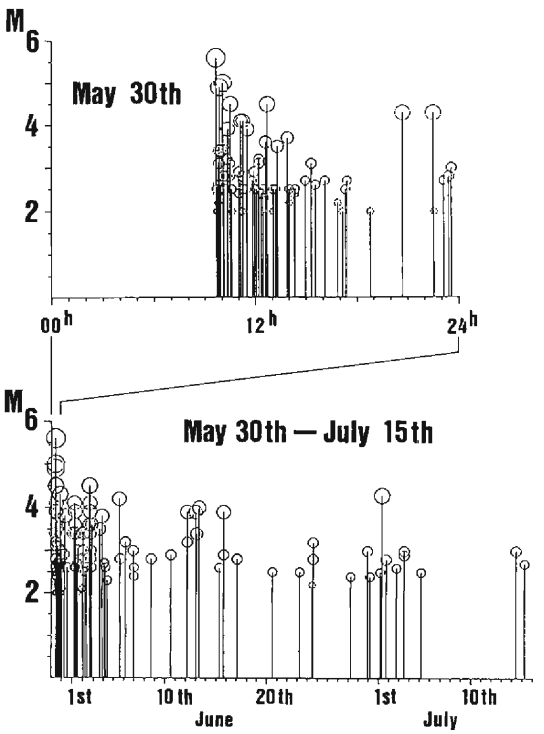

Fig. 4. Time series of the Yamasaki fault earthquake sequence in 1984[17]. The upper figure shows the precise time series of the sequence on May 30th. The lower shows the time sequence for one and a half months.

(1984)[15] and time sequence obtained by the Tottori Microearthquake Observatory[17] are shown in **Figs. 3 and 4,** respectively.

The seismic activity of the Yamasaki fault earthquake sequence is as follows: Aftershock activity was high for 8 hours just after the main shock, including six major aftershocks with magnitudes greater than or equal to 4.0. From May 31st, the aftershock activity lessened. Two days after the main shock, activity resumed and an aftershock with M4.1 occurred on June 1st as well as two events with M4.5 on June 2nd. After that, the aftershock activity decreased gradually, and aftershocks with M4.2, 4.0, 4.3 occurred on June 5th, 13th, July 1st, respectively. Since July 1st, aftershocks with magnitudes greater than or equal to 4.0 have not occurred. For earthquakes with magnitudes around 4.0, we use F–P time magnitude values obtained by the Tottori Microearthquake Observatory of Kyoto University based on an empirical formula, $M = 2.97 \cdot \log(F-P) - 2.56$[18].

3. 2 Coseismic strain steps caused by the main shock

Fig. 5 shows the strain variations recorded before and after the Yamasaki fault earthquake. Concerning the fixed–end strain, polarities of the strain steps caused by the main shock were contraction in all components except the extension in component 6–7.

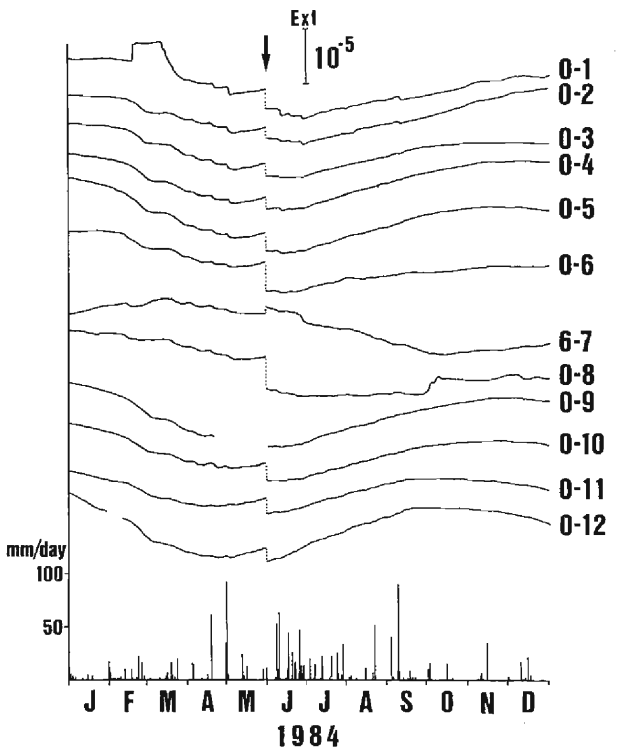

Fig. 5. Fixed-end strain variations before and after the Yamasaki fault earthquake which is indicated by the arrow. The step amplitude of component 6–7 is cut down. Daily precipitation is shown at the bottom.

Amplitudes of the strain steps range from -1.9 to -5.1×10^{-6} strain in A-tunnel and from -2.5 to -5.1×10^{-6} strain in B-tunnel, where the negative sign, "$-$", denotes contraction. Sensors No. 1 and No. 5 went off scale during the main shock and there were no data until June 1st. The step amplitude of component 6–7 was $+14.6\times10^{-6}$, where the positive sign, "$+$", denotes extension.

We compare the observed strain steps with those theoretically expected. The hypocenter coordinates obtained by Nishigami (1984)[15], fault plane solutions by Nishida (1985)[16] and magnitudes by the Tottori Microearthquake Observatory[17] are used to calculate theoretical strain steps. According to the aftershock distribution shown in **Fig. 3**, the source fault of the main shock is assumed a uni-lateral square fault of $6km \times 6$ km in area. The amount of dislocation, $D(cm)$, is obtained from an empirical formula,

$$log(D)=0.5M-1.3 \qquad \text{(Utsu (edit.) ; 1987)}^{19}.$$

P-wave velocity and Poisson's ratio are assumed to be 6.0km/sec and 0.25, respectively. The strain change before and after the earthquake is calculated by substituting these parameters into the Sato and Matsu'ura's equations[3] for a semi-infinite elastic medium. Theoretically expected strain changes are shown in **Table 2.** In this table, those for

Table 2. Theoretically expected strain changes originated by the main shock and 14 aftershocks. Three directions of N34°W N56°E and N108°E denote those of A– and B–tunnels and component 6–7, respectively. ε_1 and ε_2 mean principal strains. Azimuth is measured clockwise from the north. "+" and "−" mean extension and contraction, respectively.

No.	Y M D H Mn (Mag. by Tottori Obs.)	N34°W	N56°E	N108°E	ε_1 Amp.	ε_1 Azimuth	ε_2 Amp.	ε_2 Azimuth
						deg		deg
1	84 05 30 09h39m (M5.6)	1.31×10^{-8}	1.57×10^{-8}	6.11×10^{-8}	6.28×10^{-8}	100	-3.40×10^{-8}	10
2	05 30 09 51 (M4.9)	1.55×10^{-9}	1.55×10^{-9}	7.03×10^{-9}	7.20×10^{-9}	101	-4.10×10^{-9}	11
3	05 30 10 02 (M5.0)	5.43×10^{-9}	5.43×10^{-9}	1.94×10^{-9}	1.98×10^{-8}	101	-8.95×10^{-9}	11
4	05 30 10 30 (M4.5)	2.96×10^{-10}	1.65×10^{-10}	1.16×10^{-9}	1.17×10^{-9}	103	-7.09×10^{-10}	13
5	05 30 11 06 (M4.1)	7.67×10^{-10}	-2.09×10^{-11}	6.09×10^{-10}	7.94×10^{-10}	136	-4.62×10^{-11}	46
6	05 30 11 16 (M4.1)	1.35×10^{-10}	6.31×10^{-10}	7.08×10^{-10}	8.51×10^{-10}	85	-8.49×10^{-11}	− 5
7	05 30 12 42 (M4.5)	2.73×10^{-9}	-3.04×10^{-10}	1.84×10^{-9}	2.75×10^{-9}	141	-3.27×10^{-10}	51
8	05 30 20 43 (M4.3)	1.66×10^{-10}	-1.18×10^{-9}	4.92×10^{-10}	5.86×10^{-10}	120	-1.60×10^{-9}	30
9	05 30 22 31 (M4.3)	3.21×10^{-9}	1.09×10^{-10}	1.43×10^{-9}	3.33×10^{-9}	157	-1.26×10^{-11}	67
10	06 01 05 29 (M4.1)	3.03×10^{-10}	2.61×10^{-10}	2.63×10^{-10}	3.14×10^{-10}	171	2.50×10^{-10}	81
11	06 02 16 12 (M4.5)	6.92×10^{-10}	2.96×10^{-10}	1.81×10^{-10}	9.15×10^{-10}	177	7.30×10^{-11}	88
12	06 02 17 29 (M4.5)	8.18×10^{-10}	1.52×10^{-10}	2.40×10^{-9}	2.40×10^{-9}	106	-1.43×10^{-9}	16
13	06 06 13 47 (M4.2)	4.43×10^{-10}	2.78×10^{-10}	4.91×10^{-10}	5.01×10^{-10}	119	2.20×10^{-10}	29
14	06 13 07 00 (M4.0)	3.58×10^{-10}	6.55×10^{-11}	2.22×10^{-10}	3.60×10^{-10}	151	6.32×10^{-11}	61
15	07 01 08 02 (M4.3)	9.94×10^{-10}	-8.34×10^{-10}	-3.92×10^{-10}	1.24×10^{-9}	165	-1.08×10^{-9}	75

aftershocks are also listed. The theoretically expected strain changes for the main shock are 1.31×10^{-8} strain in A-tunnel, 1.57×10^{-8} in B-tunnel and 6.11×10^{-8} in the direction of component 6–7. The observed step polarities and theoretically expected ones are the same in component 6–7, but not so in both A- and B-tunnels. The amplitudes of the observed strain steps are about two orders of magnitude greater than the theoretical ones in the three directions. Nishigami and Tsukuda(1985)[20] obtained two kinds of fan-shaped vertical source fault with side lengths of about 5 kilometers. They also obtained the amount of dislocation ranging 8 to 14 centimeters. By adopting their parameters, the calculated strain changes become smaller than the above-mentioned values and the difference between the observed and theoretical strain step amplitudes becomes greater.

As to the partial strains, the amplitudes of strain steps are one to three orders of magnitude greater than the theoretical ones, too. The steps of partial strains in each component do not show common polarity. In the case of A-tunnel, extension and contraction distribute alternately. Such distribution of step polarities is the same as that recognized in the polarities of the secular trend of partial strain variations mentioned in part 1[9]. These phenomena show that the distribution of local strain changes are not explained by the errors of calculations or by the errors of various parameters used in calculations. These local strain changes observed in A-tunnel seem to be affected by small-scale heterogeneity of the basement of the vault. On the other hand, in B-tunnel, the two available partial strain components showed contraction. Though the polarity does not coincide with the theoretically obtained one, the two components in B-tunnel show the same polarity. Therefore, such small-scale heterogeneity confirmed in A-tunnel is not recognized in B-tunnel.

3. 3 Strain steps caused by aftershocks

The fifteen epicenters of $M\geqq4$ events of the Yamasaki fault earthquake sequence[15] are shown in **Fig. 6** with their fault plane solutions[16]. For twelve events among the fifteen, strain steps were recognized on some or most components of the extensometers. In order to calculate theoretically expected strain changes caused by aftershocks, the length of the source fault, $L(km)$, was estimated by using the empirical formula,

$$log\ (L) = 0.5M - 1.8 \qquad \text{(Utsu (edit.); 1987)}[19].$$

The ratio of the length to the width of the fault is assumed to be 2 : 1. The obtained results are shown in **Table 2. Table 3** shows the observed strain step amplitudes associated with the main shock and larger aftershocks with magnitudes greater than or equal to 4.0. As is evident from **Tables 2 and 3,** the amplitudes of the observed strain steps are usually one to two orders of magnitude greater than those theoretically expected. Concerning the aftershocks with magnitudes less than 4.0, clear strain steps were not recognized for two months after the main shock. Characteristics of the appearance of steps on the fixed-end strain components are described bellow. Each aftershock is referred to by the serial number as listed in **Table 2 or 3.** For example, event No. 1(M 5.6) is the main shock occurring at 09h39m on May 30th.

Table 3. Observed strain steps by the main shock and 14 aftershocks of M4 class. Both fixed-end strains and partial strains are listed. "sat", "NO", "×", "—" and "( )" mean overscaled data, no data, unavailable, no steps and estimated data by using micrometers, respectively.

No.	Y M D H Mn (Mag. by Tottori Obs.)	Amp. unit	0-1	0-2	0-3	0-4	0-5	0-6	6-7	0-8	0-9	0-10	0-11	0-12
1	84 05 30 09h39m (M5.6)	10^{-6}	(−3.6)	−1.9	−2.5	−2.1	(−3.4)	−5.1	15	−5.1	NO	−3.3	−2.5	−2.5
2	05 30 09 51 (M4.9)	10^{-8}	sat	−1.0	−0.82	—	sat	16	3.2	−4.7	NO	−1.9	−1.2	−1.8
3	05 30 10 02 (M5.0)	10^{-8}	sat	—	—	1.2	sat	4.9	—	−5.0	NO	−3.9	−0.50	−0.41
4	05 30 10 30 (M4.5)	10^{-8}	sat	—	—	—	sat	—	1.3	−0.74	NO	−0.22	−0.15	−0.17
5	05 30 11 06 (M4.1)	10^{-8}	sat	—	—	—	sat	—	—	—	NO	—	—	—
6	05 30 11 16 (M4.1)	10^{-8}	sat	—	—	—	sat	—	—	—	NO	—	—	—
7	05 30 12 42 (M4.5)	10^{-8}	sat	—	—	—	sat	−8.8	—	—	NO	—	—	—
8	05 30 20 43 (M4.3)	10^{-8}	sat	—	—	—	sat	−0.54	—	−1.3	NO	0.12	−0.15	−0.20
9	05 30 22 31 (M4.3)	10^{-8}	sat	—	—	0.24	sat	—	—	−0.32	NO	—	—	—
10	06 01 05 29 (M4.1)	10^{-8}	−0.13	−0.13	—	—	−0.86	−0.85	—	−1.4	—	−0.30	—	—
11	06 02 16 12 (M4.5)	10^{-8}	−1.2	−0.98	−0.79	−0.67	−1.6	−2.9	1.6	−8.0	−2.3	−1.5	−0.93	−0.93
12	06 02 17 29 (M4.5)	10^{-8}	0.23	0.48	0.22	0.41	0.21	0.98	—	—	—	−0.87	—	—
13	06 05 13 47 (M4.2)	10^{-8}	—	—	—	—	0.69	−0.44	—	−1.2	—	0.60	0.25	0.52
14	06 13 07 00 (M4.0)	10^{-8}	—	—	—	—	—	—	—	—	—	—	—	—
15	07 01 08 02 (M.3)	10^{-8}	−0.83	−0.29	−0.97	1.7	1.2	1.1	−2.2	1.4	—	0.87	1.4	2.0

(to be continued)

No.	Y M D H Mn (Mag. by Tottori Obs.)	Amp. unit	1–2	2–3	3–4	4–5	5–6	9–8	10–9	11—10	12–11
1	84 05 30 09h39m (M5.6)	10^{-6}	(−9.0)	0.64	−5.2	(3.0)	(−3.0)	×	×	−1.2	−2.4
2	05 30 09 51 (M4.9)	10^{-8}	×	−1.8	−6.1	×	×	×	×	−0.017	−3.4
3	05 30 10 02 (M5.0)	10^{-8}	×	—	−7.5	×	×	×	×	6.0	−0.18
4	05 30 10 30 (M4.5)	10^{-8}	×	—	—	×	×	×	×	-5.0×10^{-12}	−0.24
5	05 30 11 06 (M4.1)	10^{-8}	×	—	—	×	×	×	×	—	—
6	05 30 11 16 (M4.1)	10^{-8}	×	—	—	×	×	×	×	—	—
7	05 30 12 42 (M4.5)	10^{-8}	×	—	—	×	×	×	×	—	—
8	05 30 20 43 (M4.3)	10^{-8}	×	—	—	×	×	×	×	−0.65	−0.34
9	05 30 22 31 (M4.3)	10^{-8}	×	—	−1.5	×	×	×	×	—	—
10	06 01 05 29 (M4.1)	10^{-8}	−0.10	—	—	3.1	−0.87	0.073	−0.69	0.57	—
11	06 02 16 12 (M4.5)	10^{-8}	−1.7	−1.7	−1.6	2.7	−1.3	−0.95	−0.49	0.13	−0.94
12	06 02 17 29 (M4.5)	10^{-8}	−0.54	1.5	−0.99	1.1	0.013	—	−2.0	1.6	—
13	06 05 13 47 (M4.2)	10^{-8}	—	—	—	−2.5	0.99	0.28	1.4	−0.43	1.2
14	06 13 07 00 (M4.0)	10^{-8}	—	—	—	—	—	—	—	—	—
15	07 01 08 02 (M4.3)	10^{-8}	−2.5	−5.3	−4.0	3.7	1.2	−0.32	2.0	23	36

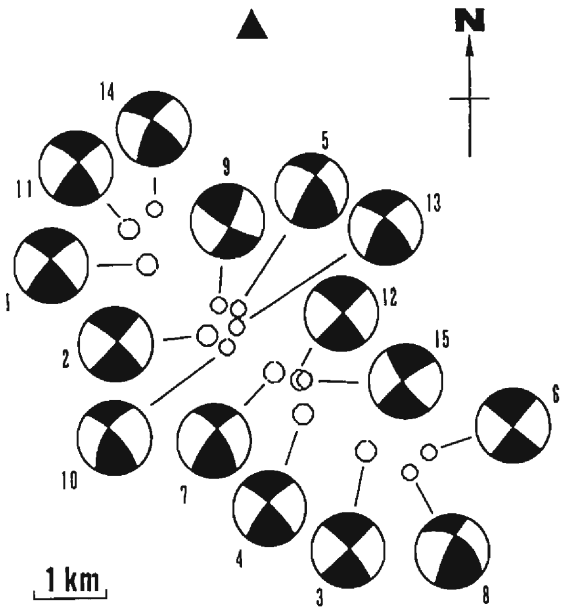

Fig. 6. Epicentral distributions of studied earthquakes ($M \geqq 4$) with fault plane solutions (upper hemisphere). The numbers correspond to those in **Table 2.** Black and white areas indicate compression and dilatation, respectively[15]. The solid triangle denotes the Yasutomi Observation Vault.

Event No. 2(M4.9) occurred twelve minutes after the main shock. All components except component 6–7 showed the same polarity of strain steps as that of the main shock. The next aftershock event No. 3(M5.0) occurred twelve minutes after event No. 2. The strain step amplitudes of this aftershock were, in spite of being of comparable magnitude, a few times smaller than those of the previous one of M4.9, except for component 0–10. The third aftershock event No. 4(M4.5), which occurred twenty–eight minutes later, showed small steps on component 6–7 and all components in B–tunnel, except the two unavailable ones. After this, no strain steps were recognized during two aftershocks, event No. 5(M4.1), event No. 6(M4.1). **Fig. 7** shows the relation between the time sequence of aftershocks and the averaged strain step amplitudes with their absolute values. From this figure, concerning five aftershocks with magnitudes greater than 4.0 for two hours from the main shock to event No. 6, it is generally said that the amplitudes of strain steps depend on the magnitudes of earthquakes and also decrease with time.

After a quiescent period of one and half hours, the next aftershock with magnitude greater than 4.0, event No. 7(M4.5), occurred. Eight hours later, event No. 8(M4.3) occurred. Some extensometer components showed small but clear steps from those aftershocks. A succeeding aftershock event No. 9(M4.3), however, produced no strain steps.

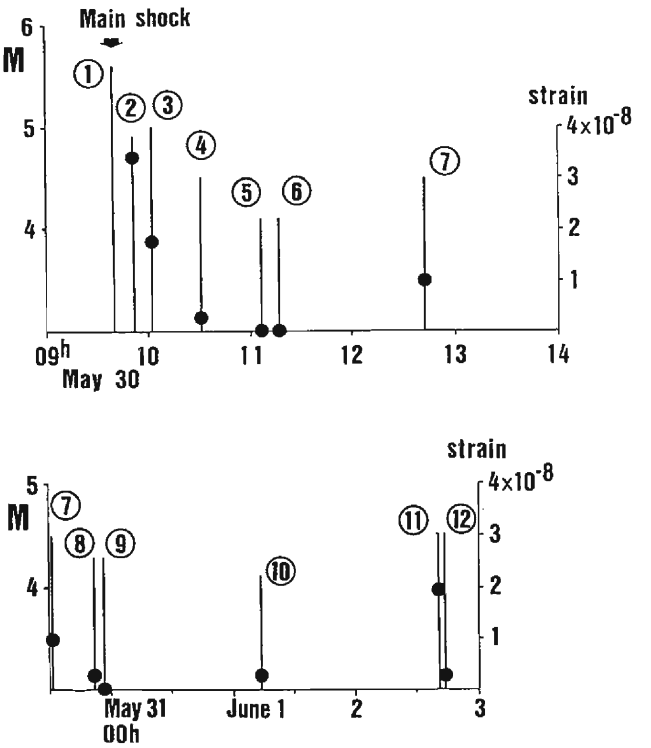

Fig. 7. Aftershock sequence and the averaged amplitudes of observed strain steps in absolute values (solid circles). The numbers correspond to those in **Table 2.**

Both events No. 10(M4.1) and No. 11(M4.5) occurred after quiescent periods of one and half days and produced clear strain steps. It is noteworthy that comparatively large strain steps were observed by aftershocks which occurred after some quiescent periods.

Just after event No. 11, another aftershock event No. 12(M4.5) occurred successively. The strain steps of event No. 12(M4.5) are a few times smaller than those of event No. 11. In **Fig. 7**, four pairs of aftershocks are seen, namely, events No. 2 and No. 3, No. 5 and No. 6, No. 8 and No. 9, No. 11 and No. 12. In three cases of these four pairs, strain step amplitudes of the former events are larger than those of the latter ones. Therefore, it can be said that comparatively large strain step amplitudes are caused only by the former event of each pair.

Event No. 13 occurred after a quiescent period of three days. For this aftershock, it was noticeable that some components showed step polarities opposite to those of the main shock. No strain steps were recognized during event No. 14(M4.0). This may be because of the fact that event No. 14 is the smallest aftershock in this analysis, and perhaps was too small to cause any strain steps.

A half month later, event No. 15(M4.3) occurred. Remarkable strain steps were observed from this aftershock. Nevertheless, the step polarities of most components were opposite to those of the main shock.

Summarizing the above, it can be said that if an aftershock with magnitudes greater than 4.0 occurs after some quiescent period, some amount of strain steps can be expected.

3. 4 Polarities of principal strain axes derived from strain steps

In part 1[9], we investigated the directions of principal strain axes, ε_1–and ε_2–axes, for long–term strain variations employing two combinations of extensometers, 0–3, 0–10, 6–7 on the northern side of the main fractured zone (called N–combination), and 0–2, 0–11, 6–7 across the main fractured zone (F–combination). It was concluded in part 1[9] that the Yasutomi fault zone had changed in thickness with intervals of a few years. In this section, we have obtained the principal strains of steps and examined the change of thickness by using the same extensometer combinations as mentioned above.

As for the main shock, almost the same principal strain axes were obtained for N– and F–combinations. One principal strain axis, ε_1, was a contraction of $1.9\sim2.6\times10^{-5}$ strain in N11$\sim$12°E, and the other, ε_2, was an extension of 1.5×10^{-5} strain in E11$\sim$12° S. In other words, the contraction was almost normal to the fault and the extension was almost parallel to it. The results are shown in **Fig. 8.** The strain releasing pattern of both combinations and that theoretically expected are almost the same. However, the observed amplitudes of strain released are more than two orders of magnitude greater than the theoretical one.

Among the aftershocks listed in **Table 3,** only strain steps of event No. 11 and event No. 15 were large enough to calculate principal strains with good accuracy for both N– and F–combinations. Their principal axes are illustrated in **Fig. 9** with those theoretically expected.

Concerning the former event No. 11, the directions of ε_1 for N– and F–combinations are E22°S and E11°S, respectively, and are almost parallel to the fault zone. Their amplitudes are 1.6×10^{-8} and 1.7×10^{-8}, respectively. ε_2 for N– and F–combinations are normal to the fault and the amplitudes are 3.9×10^{-8} and 3.6×10^{-8}, respectively. Although these amplitudes are about two orders of magnitude smaller than those of the main shock, the directions of principal axes are almost the same as those of the main shock.

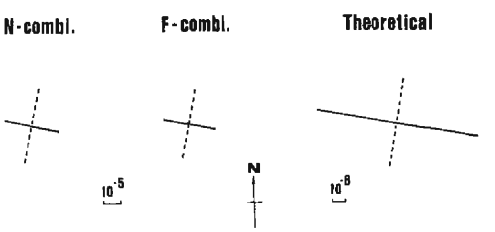

Fig. 8. Horizontal principal strains for the main shock derived from the observed strain steps and those calculated theoretically. N–combi. and F–combi. mean both combinations of three components, (0–3, 0–10, 6–7) and (0–2, 0–11, 6–7), respectively. Solid lines and broken lines denote extension and contraction, respectively.

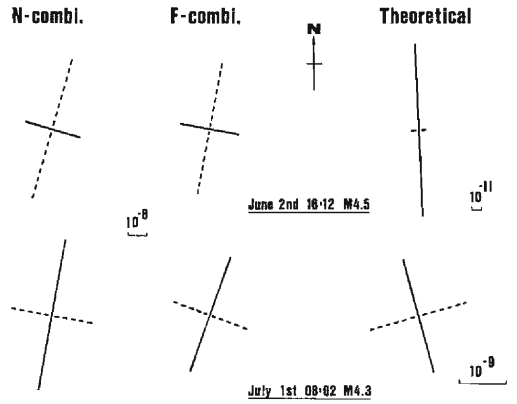

Fig. 9. Principal strains for two major aftershocks, events 11 and 15. Notations are the same as those in **Fig. 8.**

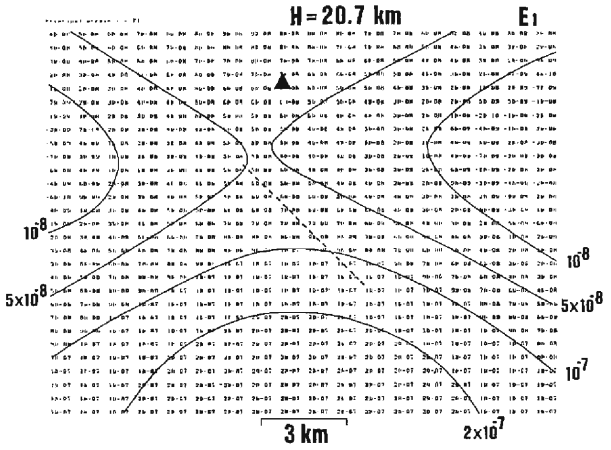

Fig. 10a. Amplitude distribution of principal strain ε_1 for the Yamasaki fault earthquake. Broken line denotes the assumed fault and solid triangle, the Yasutomi Observation Vault.

For the latter event No. 15, one principal strain axis, ε_1, was extension in the directions of N20°E and N11°E with amplitudes of 4.1×10^{-8} and 3.2×10^{-8} strain for N– and F–combinations, respectively. The other principal strain axis, ε_2, was contraction with amplitudes of 2.3×10^{-8} and 2.2×10^{-8} strain for N– and F–combinations, respectively. The polarities that the extension normal to the fault and contraction parallel to it are almost reverse to those of the main shock and the former aftershock. However, it is noticeable that, in spite of their polarities, the azimuths of principal strain axes were normal and parallel to the fault zone.

On the other hand, most of the theoretical strains for the aftershocks show extension

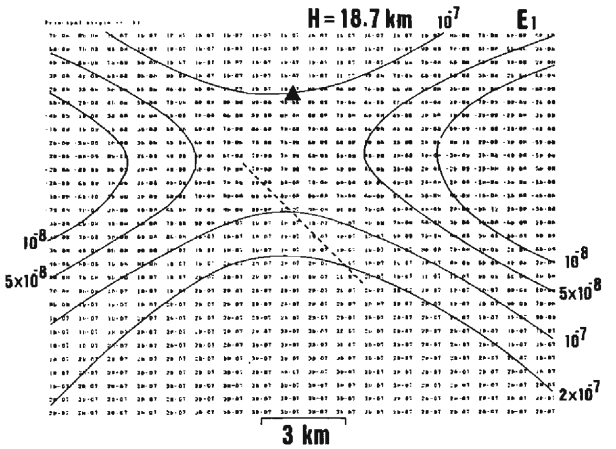

Fig. 10b. Amplitude distribution of principal strain ε_1 for an assumed earthquake whose hypocenter is 2 km shallower and shifted 0.5 km toward NW direction from that of the Yamasaki fault earthquake. Other parameters are the same as in **Fig. 10a.**

from E–W to NW–SE. As the hypocentral distances are short, the amplitudes and directions of principal strain considerably depend on the hypocenter location. **Figs. 10 a and b** show ε_1 for two different cases of hypocentral locations. Other allowable adjustment of hypocentral parameters cannot reduce the discrepancies between theory and observation. Therefore, the distribution of strain changes also strongly depends on local heterogeneity.

4. Strain steps originated by distant earthquakes

Coseismic strain steps are sometimes caused by distant earthquakes. However, there are also many cases where no strain steps are caused even by large distant earthquakes. From the minute data stored on CMT, distant earthquakes which originated strain steps are listed in **Table 4.** In this section, strain steps related to such distant earthquakes are discussed.

4. 1 Principal strain axis of the strain steps

The strain step data saved by the CMT recorder were analyzed. Principal strains were calculated when strain steps of at least two directions were observed for both N– and F–combinations. The results for both combinations are shown in **Fig. 11.** The directions of principal axes are also mostly distributed normal or parallel to the fault strike, so that they seem to support the idea of thickness change of the fault zone. Especially, the principal strain axes obtained by N–combinations depend much more on the fault strike than those of F–combinations. This tendency is quite similar to that recognized for long–term strain variations shown in part 1[9].

One hour after the earthquake of M6.5 off Fukushima (event No. 20 in **Table 4**),

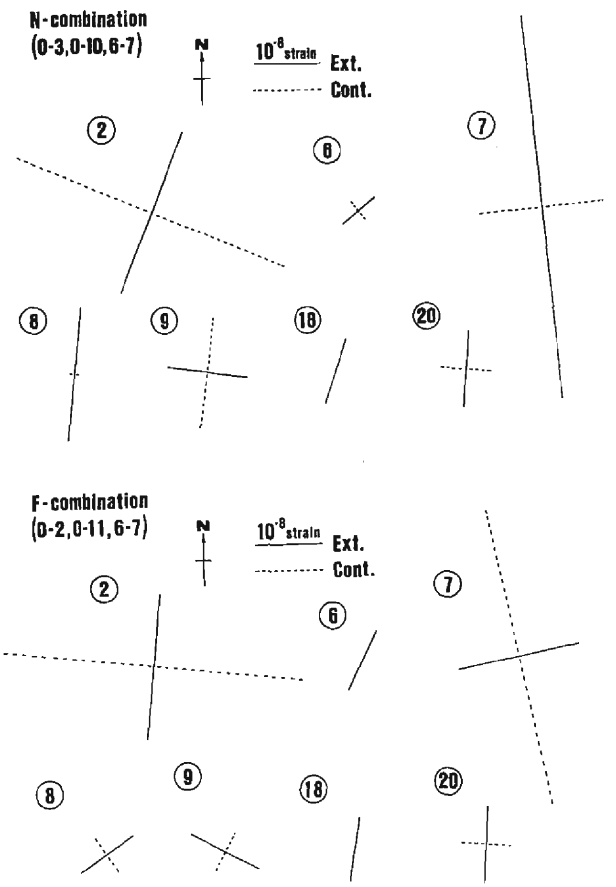

Fig. 11. Principal strains derived from the strain steps caused by distant earthquakes. The upper figure shows those derived from N–combination and the lower figure, F–combination. The numbers correspond to those in **Table 4.**

another earthquake of M6.7 occurred successively at almost the same locations. Nevertheless, no strain steps were observed by the latter earthquake. Such phenomenon in which a large strain step is caused by the first event of temporally clustered earthquakes is quite the same as that recognized in the case of the Yamasaki fault earthquake sequence.

4. 2 Magnitude, epicentral distance and strain steps

The strain steps which are originated by distant large earthquakes and recorded by the monitor recorder are discussed. Strain steps of greater than 5×10^{-9} strain are detectable by the monitor recorder. In order to know what kind of distant earthquakes originate strain steps at the Yasutomi Observation Vault, earthquake data of three categories were chosen from the J.M.A. catalogue and examined as to whether corresponding strain steps were observed or not on the monitor records. The selected

Table 4. List of strain steps originated by distant earthquakes. "—", "×", "?" and "—?" mean no steps, unavailable, doubtful and probable contraction, respectively.

No.	Y M D H Mn (JMA Mag.) Region depth	Amp. unit	0–1	0–2	0–3	0–4	0–5	0–6	6–7	0–8	0–9	0–10	0–11	0–12
1	81 6 30 06h26m (M3.1) E. Chugoku 10km	10^{-6}	—	—	1.5?	—	—	—?	—	—	—	—	—	—
2	83 10 31 01h51m (M6.2) C. Tottori 15km	10^{-6}	4.2	−4.0	11	17	5.2	−21	−22	—	2.5	2.0	−8.2	−9.2
3	83 10 31 14h40m (M5.4) Hokkaido 262km	10^{-6}	2.2	—	—	—	1.7	—	—	—	—?	—	—	—
4	83 11 15 12h12m (M3.1) Osaka Bay 14km	10^{-6}	1.3	—	—	—	—	—	—	—	—	—	—	1.5
5	83 11 16 05h13m (M3.8) N. Kinki 17km	10^{-6}	—	—	—	—	—	—	—	−6.6	—	—	—	—
6	84 01 01 18h03m (M7.3) Off Kii Pen. 388km	10^{-6}	—	1.0	−1.4	−2.4	−1.2	—	—	—	2.0	3.1	3.4	2.7
7	84 08 07 04h06m (M7.1) Hyuganada 33km	10^{-6}	−2.3	−18	21	34	20	14	1.6	5.0	4.6	4.3	4.8	7.3
8	84 09 14 08h48m (M6.8) W. Nagano 2km	10^{-6}	−2.7	−3.0	5.6	9.2	6.5	−1.4	—	—	×	4.1	4.9	5.7
9	85 01 06 00h46m (M5.9) Wakayama 70km	10^{-6}	—	4.1	−1.8	−5.3	−3.2	—	5.8	×	−1.5	—	−1.1	−1.8
10	85 04 03 09h58m (M3.5) Yamasaki 15km	10^{-6}	—	—	—	—	—	—	—	−3.3	−1.3	−2.7	−2.5	−5.8
11	85 04 04 05h21m (M6.6) Ogasawara 458km	10^{-6}	—	—	—	—	—	—	—	—	—	—	1.8	—
12	85 05 13 17h05m (M4.1) Hyuganada 29km	10^{-6}	—	—	—	—	—	—	5.7?	—	—	—	—	—
13	85 05 13 19h41m (M6.0) Ehime 39km	10^{-6}	—	—	—	—	—	—	—	—	—	1.7	1.0	3.0
14	85 05 29 15h10m (M2.8) S. Kii Pen. 49km	10^{-6}	—	—	—	—	−1.0	−2.3	—	—	—	—	—	—
15	85 10 22 07h48m (M4.6) Harimanada 13km	10^{-6}	—	—	—	—	—	5.6?	—	—	—	0.68	—	—
16	85 11 27 09h01m (M5.1) Obama 11km	10^{-6}	—	1.2	—?	—	−2.6	—	—	—	—	—	—	—
17	86 03 22 17h26m (M3.0) SE. Hyogo 17km	10^{-6}	−0.64	—	—	—	—	—	—	—	—	—	—	—
18	86 06 24 11h53m (M6.5) Off Boso Pen. 73km	10^{-6}	2.0	2.5	1.9	1.1	1.9	—	—	—	2.3	2.9	2.3	3.5
19	86 07 28 22h39m (M4.2) Oki is. 21km	10^{-6}	—	—	—	—	—	2.9	—	—	—	—	—	—
20	87 02 06 21h23m (M6.4) Off Fukushima 30km	10^{-6}	—	2.0	1.6	1.5	—	—	−3.3	—	—	—	—	—
21	87 03 18 12h36m (M6.6) Hyuganada 48km	10^{-6}	—	2.3	−2.5	−2.0	−1.6	−2.5	—	—	—	—	—	—
22	88 07 31 08h40m (M5.2) Izu Pen. 5km	10^{-6}	—	2.4	—	2.8	—	—	—	—	—	—	—	—
23	89 02 19 13h58m (M5.3) N. Mie 45km	10^{-6}	—	1.1	—	—	—	—	—	—	—	—	—	—

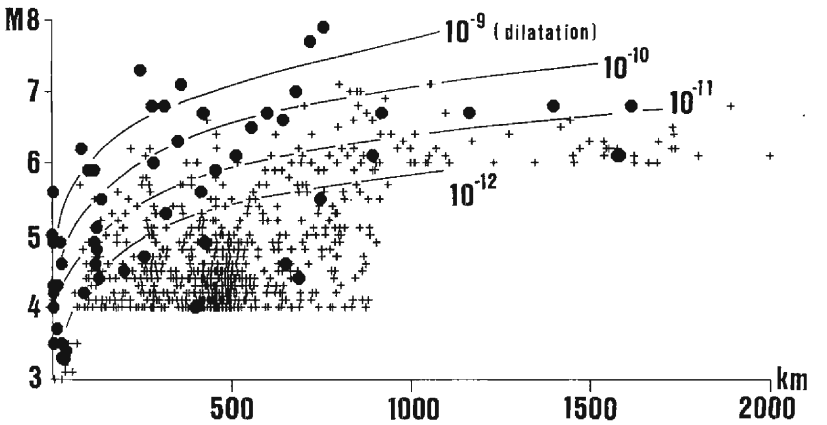

Fig. 12. Magnitudes and epicentral distances of earthquakes analyzed. Solid circles denote the earthquakes by which at least one component of strain step is recognized by the monitor recorder. Cross marks denote the earthquakes with no strain steps. Curves show maximum dilatations for reference which are theoretically expected to be generated by the earthquakes of fifteen kilometers deep in semi-infinite elastic medium.

earthquakes were (a) earthquakes with $M \geqq 6$ in and around the Japan Islands, (b) earthquakes with $M \geqq 4$ in Southwest Japan and (c) earthquakes with $M \geqq 3$ around the Yamasaki fault. These criteria were adopted from our experiences as the level of the smallest earthquake which causes the strain steps at the Yasutomi Observation Vault. Concerning these earthquakes, when corresponding strain steps are recognized by at least one component, the earthquake is considered to trigger strain steps. In **Fig. 12**, all earthquakes examined are plotted on the Magnitude-Epicentral distance space. Cross marks denote the earthquakes associated with no strain steps and circles denote those which originated strain steps. Maximum dilatations expected from crustal earthquakes of fifteen kilometers deep are shown on the figure for reference, which are theoretically calculated by using Sato and Matsu'ura's method[3] for a semi-infinite elastic medium. As the detectability of the monitor recorder is 5×10^{-9} strain, the amplitudes of observable strain steps should be greater than 5×10^{-9} strain. Strain steps with amplitudes greater than 5×10^{-9} are occasionally recognized for some earthquakes, in spite of the fact that the corresponding strain steps with such large amplitudes cannot be expected theoretically. Consequently, in the case of our observations, it can be said that most observed strain steps are neither explained theoretically nor agree with the existing empirical models.

4. 3 Seasonality of the strain step direction

If the released strain by strain steps is greater than the theoretically expected one, the energy source that provides such an amount of strain may be the tectonic stress and/or due to meteorological effects. In order to examine whether the meteorological phenomena affect or not, we investigated the seasonal variation of strain step amplitudes. **Fig. 13** shows the relation between the strain step data saved by the CMT recorder and

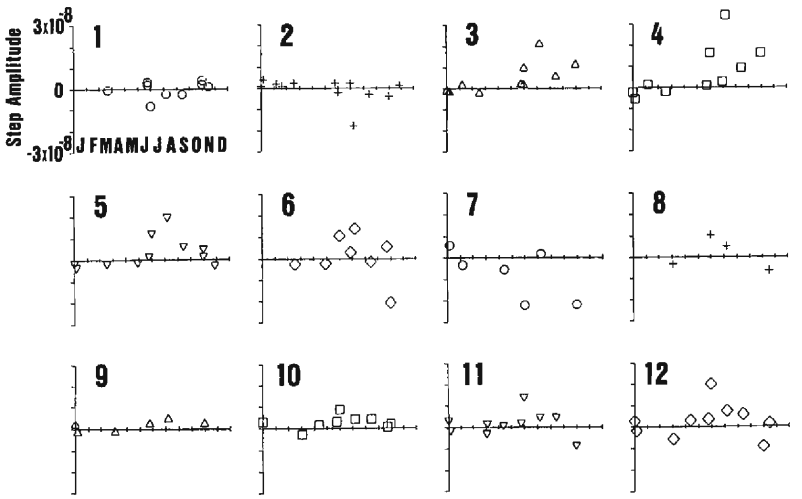

Fig. 13a. Seasonal distribution of amplitudes of strain steps saved by CMT recorder.

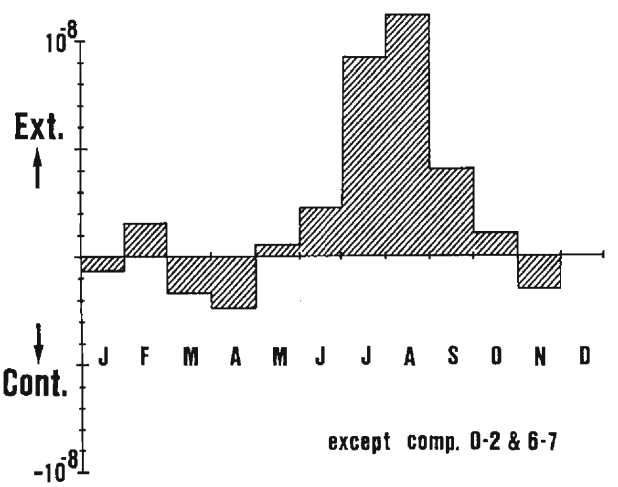

Fig. 13b. Monthly average of strain steps except components 0–2 and 6–7.

the month of the earthquake occurrence which originated those strain steps. From this figure, some seasonality can be recognized, namely, extending steps are dominant from May to November, and contracting ones, from December to April, except for components 0–2 and 6–7. As mentioned in part 1[9], annual strain variations show extension (differential coefficients are positive) from May to November and contraction (those are negative) from December to April. These annual strain variations are caused by the annual variation of surface temperature. Accordingly, it can be said that the polarities of strain steps caused by distant earthquakes are closely related to the annual strain

variations.

Two components, 0–2 and 6–7, show a noticeable tendency reverse to the other components. The reverse tendency of component 0–2 is suggestive. Generally speaking, the fractured zones inside the fault zone mutually affect each other, and the behavior of the fault zone itself is considered to be the composite phenomenon of the behaviors of these fractured zones. The reverse tendency of component 0–2 is considered to be caused by the highly fractured zone near sensor No. 2.

5. Characteristics of the observed strain steps

The characteristics of the observed strain steps given in sections 3 and 4 are summarized in the following:

(1) The amplitudes of the strain steps originated by earthquakes are frequently one to two orders of magnitude greater than those theoretically expected. The step polarities frequently do not coincide with theoretically expected ones either.

(2) The strain steps originated by earthquakes after a quiescent period are usually large, while strain steps originated by successive earthquakes are frequently small.

(3) No simple relation among the recorded amplitudes of strain steps, the magnitude of earthquake and the epicentral distance has been found in the case of the Yasutomi Observation Vault.

(4) The directions of principal axes of strain steps mean the strain variation in the direction normal to the Yasutomi fault zone.

(5) The strain steps originated by distant earthquakes show some seasonal variations in their polarities. This seasonality is consistent with the annual strain variations.

(6) The step polarities of component 0–2, which is adjacent to the fractured zone, also show some seasonality, but, these polarities are in opposite direction to those of the other components.

From these results, the following interpretations can be presented. The released strain by strain steps triggered by seismic waves is mainly that which has been previously accumulated around the observation site. Therefore, the amplitudes of strain steps depend on the condition of strain accumulation at the observation site. Taking account of the shallowness of the vault and the seasonality of step polarities mentioned above, this locally accumulated strain is considered to be produced by the annual variations of surface temperature. The pattern by which this pre-accumulated strain is released is controlled by the fractured zones in the area where the thermal stress has been accumulated. In the next section, we will present a mechanical model which explains these characteristics of the observed strain steps.

6. A simulation of strain variations by a mechanical model

6. 1 Construction of the model

Many kinds of simple mechanical models which consist of springs, sliders and dashpots have been presented to explain earthquake related phenomena in the crust. Movements of the source fault are usually expressed by stick slips of sliders[21)~25)]. The

main purpose of making such mechanical models is to get a clue of the successive steps in unsolved crustal movements by expressing known crustal activities with simple constituent elements. In this section, we present a simple mechanical model which simulates the processes by which temperature variations accumulate strain locally, and by which that strain is released.

As a model of the basement rock of the observation site, we consider a structure where many material points are combined three-dimensionally by sliders and elastic springs. The two-dimensional section of this structure is illustrated in **Fig. 14.** Each spring has its own elastic constants. Each slider also has its own static and dynamic frictional coefficients for shear movement, but is treated as an coherent body for normal movement. A slender rectangular area surrounded by a dotted line in the figure corresponds to the observation site and each material point corresponds to each displacement sensor. We consider the case in which the stress is applied only in the direction of the length of this slender area. Shear stress is then generated between the area and the neighboring portions, but without normal stress. Only frictional force caused by the shear stress need be considered. Therefore, the springs normal to the slender area may be replaced by bar springs. The mechanical model shown in **Fig. 15** represents the behavior of this slender area under these circumstances. Elements adjacent to the slender area in **Fig. 14** correspond to the floor in **Fig. 15.**

In this model, material points, m_i $(i=1\sim n)$, are combined by helical springs longitudinally. Both ends of the system are connected at a great distance to walls through weak helical springs. Strain is defined by dividing the relative displacement between two neighboring material points by the initial length of the helical spring. The Young's modulus of each helical spring, k_i, can take an arbitrary value. The Young's modulus of each fractured zone is assumed to be smaller than those of other portions. Each material point is connected to the adjacent slender area through a bar spring and a slider. The rigidity of each bar spring is denoted by l_i. The static and dynamic frictional coefficients of each slider are denoted by μ_i^0 and μ_i, respectively.

A bar spring transfers the weight of a material point to a slider and originates the frictional force, independent of its deformation. There are two major characteristics con-

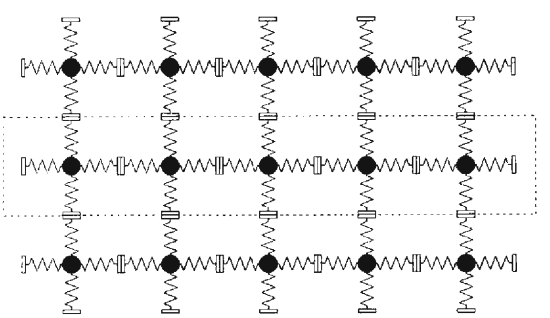

Fig. 14. Schematic structure of the basement rock.

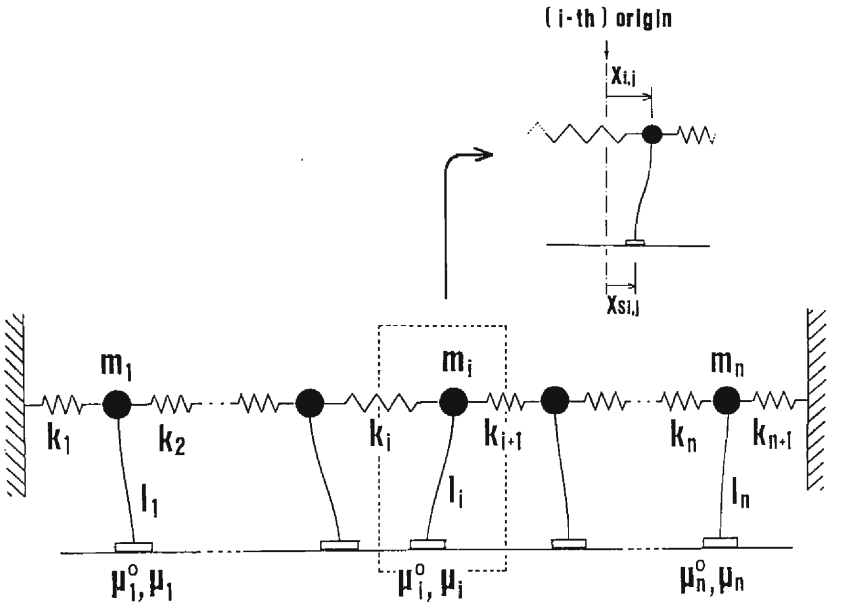

Fig. 15. A mechanical model which represents the structure of the basement rock shown in Fig. 14. Displacements x_i and x_{si} are defined in the figure.

cerning this model. One is that each helical spring is subjected to thermal deformation with a linear coefficient for thermal expansion, β, and therefore the length of a helical spring varies in proportion to temperature variations. The other is that the movements of sliders do not correspond directly to strain steps but the movements of sliders affect the locations of material points and yield the strain changes between them. The coefficient, β, and the initial length of a spring, L_0, at temperature T_0 are assumed to be the same throughout all springs. Therefore, the length, L, of a spring at temperature $T=T_0+\Delta T$ is

$$L=L_0\,(1+\beta\cdot\Delta T)\,, \tag{1}$$

where ΔT is temperature variation. Elastic constant, k_i, is assumed not to be changed by the temperature variation. When an external force is applied to a helical spring and consequently extensional strain in the spring is generated, this is defined as positive strain. Corresponding to this extensional strain, tensile stress is generated in the spring. The direction of this stress is defined as positive. Furthermore, if the temperature varies by ΔT, the relation between stress (σ) and strain (ε) of the helical spring is

$$\sigma=k\cdot\varepsilon-k\cdot\beta\cdot\Delta T. \tag{2}$$

If the both ends of the spring are fixed, namely $\varepsilon=0$,

$$\sigma = -k \cdot \beta \cdot \Delta T. \tag{3}$$

When temperature increases, as seen in equation (2), the compressive stress increases within the spring. If the temperature does not change, namely $\Delta T=0$, equation (2) expresses Hooke's Law.

In the following, x_i and x_{si} denote the displacements of each material point and those of each slider, respectively(**Fig. 15**). The origins of the locations are the initial equilibrium positions of each material point and slider, where the stress of each portion is zero at $t=0$.

Let us consider the case when temperature variation ΔT is applied uniformly to the system shown in **Fig. 15**. All helical springs tend to be thermally deformed, causing each material point to move, depending on the elastic constants, Young's modulus k_i and rigidity l_i. Strain energy accumulates within the helical and bar springs, and all material points stop at their new equilibrium positions. Each bar spring then acquires a restoring force of $x_i \cdot l_i$. If this restoring force exceeds the static frictional force of $m_i \cdot \mu_i^0$, the slider starts moving in the direction in which the restoring force decreases, and stops at the point where the restoring force becomes equal to the dynamic frictional force of $m_i \cdot \mu_i$. Consequently, the restoring force of the bar spring decreases, inducing the equilibrium position of all material points to change, as do the restoring forces of all the bar springs. If newly acquired restoring force exceeds the static frictional force again, the same process is repeated.

The above behavior of the model can be expressed by the following equations. At time $t=t_j$, the temperature of the system becomes $T=T_j$, and the locations of each material point and slider are $x_{i,j}$ and $x_{si,j}$, respectively.

As the extension of the i+1–th helical spring is $(x_{i+1,j}-x_{i,j})$, the contracting force, ΔF, of this spring becomes

$$\Delta F_{i+1,j} = k_{i+1}(x_{i+1,j}-x_{i,j}) - k_{i+1} \cdot \beta \cdot L_0(T_j - T_0). \tag{4}$$

Similarly, the contracting force of the i–th helical spring is

$$\Delta F_{i,j} = k_i(x_{i,j}-x_{i-1,j}) - k_i \cdot \beta \cdot L_0(T_j - T_0). \tag{5}$$

As the restoring force of the bar spring is

$$-l_i(x_{i,j}-x_{si,j}), \tag{6}$$

the same force acts on the slider. Consequently, the equilibrium equation for the i–th material point is

$$\Delta F_{i+1,j} - \Delta F_{i,j} - l_i(x_{i,j}-x_{si,j}) = 0, \tag{7}$$

where the right direction is taken as positive. By rewriting equation (7), we get

simultaneous linear equations,

$$k_{i+1} \cdot x_{i+1,j} - (k_{i+1} + k_i + l_i) x_{i,j} + k_i \cdot x_{i-1,j} = \beta \cdot L_0 (T_j - T_0)(k_{i+1} - k_i) - l_i \cdot x_{si,j} \qquad (i = 1 \sim n). \tag{8}$$

As the both ends are fixed, x_0, x_{s0} and x_{n+1} are equal to 0 in linear equations (8). The static frictional force of $m_i \cdot \mu_i^0$ between the floor and the i-th slider prevents the slip of the slider. If any restoring force obtained by solving linear equations (8) exceeds the corresponding static frictional force,

$$| -l_i(x_{i,j} - x_{si,j}) | > m_i \cdot \mu_i^0, \tag{9}$$

the slider starts sliding towards the decrease in restoring force. And when the restoring force decreases and equilibrates with the dynamic frictional force,

$$| -l_i(x_{i,j} - x_{si,j}) | = m_i \cdot \mu_i, \tag{10}$$

the slider stops moving. Corresponding to the changes of bar spring restoring force, the equilibrium positions of all material points are rearranged. This rearrangement also causes the changes of strain energy within the helical springs and the bar springs. Therefore, linear equations (8) should be solved again by substituting those slider locations, $x_{si,j}$, obtained by equation (10). If the restoring forces of all bar springs do not exceed static frictional forces of the corresponding sliders, all material points are set to their equilibrium locations.

The change in strain is obtained by dividing the change of relative distance between two material points by the initial length of the spring involved,

$$\Delta\varepsilon_{i,j} = (x_{i,j} - x_{i-1,j})/L_0 . \tag{11}$$

In the practical calculations for the present simulation, all the values of the above parameters are assumed a priori and the temperature variations are given by a sinusoidal function. For example, by taking 1/180 of the sinusoidal change as a unit time step, the equilibrium locations of all material points were obtained for each time step.

All material points included in the system can suddenly be moved from their locked position upon the arrival of seismic waves. In order to express this situation, we assume that the static frictional coefficients μ_i^0 drop to 10% of their originally assumed values only at the time instant of seismic wave arrival.

By this decrease of static friction, sliders temporarily become easy to move. Here, the dynamic frictional coefficients μ_i are also assumed to decrease to 10% of their original values to represent stress drops at each material point. The strain variations of the components related to the moved sliders are generally greater than when they don't move. In other words, appreciable strain changes are recognized as strain steps in the present simulations. At the next time instant after the seismic wave arrival, both static

and dynamic frictional coefficients are assumed to recover their original values, and each element tends to stabilize, depending on their parameters.

6. 2 Numerical calculations and results of simulations

Some numerical simulations were carried out by using the above mechanical model with twelve material points in one direction. This model aims to simulate the general features of strain variations in a heterogeneous field. All material points and helical springs have the same mass and the same initial length, respectively. k_i, l_i, μ_i^0 and μ_i are given by using random number tables. We consider that the non-uniform elastic constants will express the extent of fracture of the basement rock. In this article, calculations are carried out employing two kinds of parameter sets, A-group and B-group. The parameters used are listed in **Table 5.**

Annual temperature variations, $T(t)$, are given by a sinusoidal function, $T(t)=T_0+T_a\sin(\omega t+\delta_0)$, where T_0 and T_a are the initial temperature and the amplitude of temperature variations, respectively. In this case, one cycle of $T(t)$ is divided into 180 time steps; therefore, a time interval becomes $2\pi\omega/180$, which corresponds to about two days. Numerical calculations are carried out at this time interval. The results obtained are the strain variations between two neighboring material points, which correspond to partial strain variations. The results are shown in **Figs. 16, 17 and 18.**

Fig. 16 shows the strain variations which are originated by one cycle of temperature variations. This one cycle can be considered as annual variations with no earthquakes occurring during this one year period. The amplitudes of strain variations differ for each component. Generally speaking, the portions with small Young's modulus k_i tend to show small amplitudes of annual strain variations.

Fig. 17 shows the seasonal variations of strain step polarities. Earthquakes are generated every month (shown by dotted lines in the figures) and the polarities of strain steps by those earthquakes are examined. For almost all components, extensional steps are recognized when annual strain variations tend to increase, and vice versa. However, there are some components which show the reverse polarity. Generally speaking, strain steps are small when variation rates of strain are small.

Figs. 18a and b show the amplitudes of strain steps by five sets of two successively occurring earthquakes with time intervals of 2/3, 4/3, 2, 8/3 and 10/3 days, respectively. **Fig. 18a** represents strain variations with positive differential coefficients and **Fig. 18b** is for the negative case. From these figures, the strain steps by the latter earthquake is not obvious when the time interval is 2/3 days. In contrast, when two earthquakes occur with a time interval of 10/3 days, strain steps with almost the same amplitude can be observed in both earthquakes. Furthermore, we can recognize some strain steps originating with no external seismic waves. The surrounded area in **Fig. 18a** is enlarged and illustrated in **Fig. 18c** to show small strain variations clearly. Zigzag variations recognized in the figure are caused by small steps of sliders without external seismic waves. We call these small steps non-seismic steps.

From **Figs. 16, 17 and 18,** the following characteristics are confirmed.

(1) The amplitudes of annual strain variations vary with elastic constants (**Fig. 16**).

Table 5. Parameter list used in the simulations. K_i and L_i of elastic constants denote Young's modulus of each helical spring and rigidity of each bar spring, respectively. μ_i^0 and μ_i of frictional coefficients mean static and dynamic frictional coefficient of each slider, respectively.

Common parameters	
Number of material points	12
Mass of a material points	2.6×10^4 gr.
Initial length of a helical spring	1000cm
Initial temperature	15℃ (deg.)
Amplitude of temperature variations	1.5℃
Line coefficient of thermal deformation	5×10^{-6} deg.$^{-1}$

A-group :

	Elastic const.		Frictional coeff.	
No.	Young's modulus K_i	rigidity L_i	static μ_i^0	dynamic μ_i
1	1.20×10^{11}	1.50×10^{11}	.40	.30
2	2.31	1.95	.38	.26
3	2.61	1.53	.43	.21
4	2.28	1.77	.38	.25
5	2.58	1.80	.43	.25
6	2.61	1.83	.44	.21
7	2.64	2.07	.44	.28
8	2.49	1.92	.42	.21
9	2.55	2.04	.43	.28
10	2.22	1.74	.37	.29
11	2.64	2.10	.44	.23
12	2.16	1.95	.36	.21
13	1.32	—	—	—

B-group :

	Elastic const.		Frictional coeff.	
No.	Young's modulus K_i	rigidity L_i	static μ_i^0	dynamic μ_i
1	1.28×10^{11}	2.10×10^{11}	.56	.41
2	2.97	2.10	.54	.49
3	2.76	2.37	.51	.45
4	2.58	2.07	.56	.47
5	2.61	2.31	.62	.49
6	2.61	2.04	.62	.49
7	2.55	1.95	.58	.47
8	2.76	2.04	.61	.47
9	2.64	2.22	.54	.45
10	2.28	2.07	.59	.44
11	2.49	2.25	.56	.48
12	2.37	1.89	.51	.48
13	1.26	—	—	—

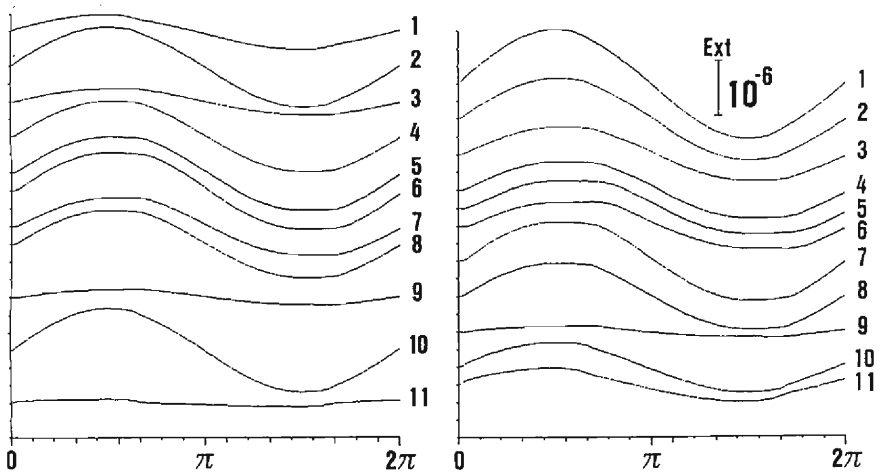

Fig. 16. Strain variations originated by the temperature variations of one cycle calculated from the mechanical model. The left figure corresponds to A–group in **Table 5**, and the right one, to B–group.

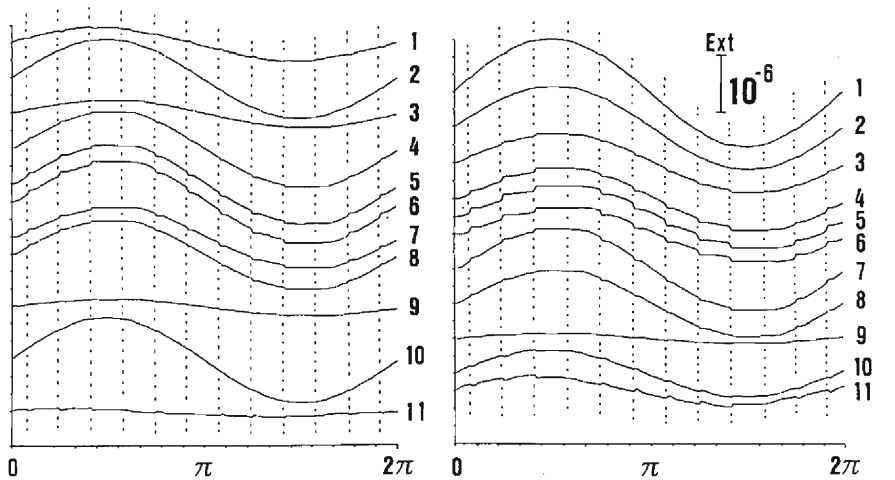

Fig. 17. Strain variations originated by the temperature variations of one cycle calculated from the mechanical model in the case where twelve earthquakes are generated every month. The left figure corresponds to A–group in **Table 5** and the right one, to B–group.

(2) Extensional strain steps predominate in the period when the differential coefficient of strain variation is positive, and vice versa. This indicates that seasonality of strain variations governs the polarities of strain steps (**Fig. 17**).

(3) Reverse relation between differential coefficients of strain variations and step polarities is occasionally recognized (**Fig. 17**). This may be caused by the mutual relation among elastic constants of neighboring springs.

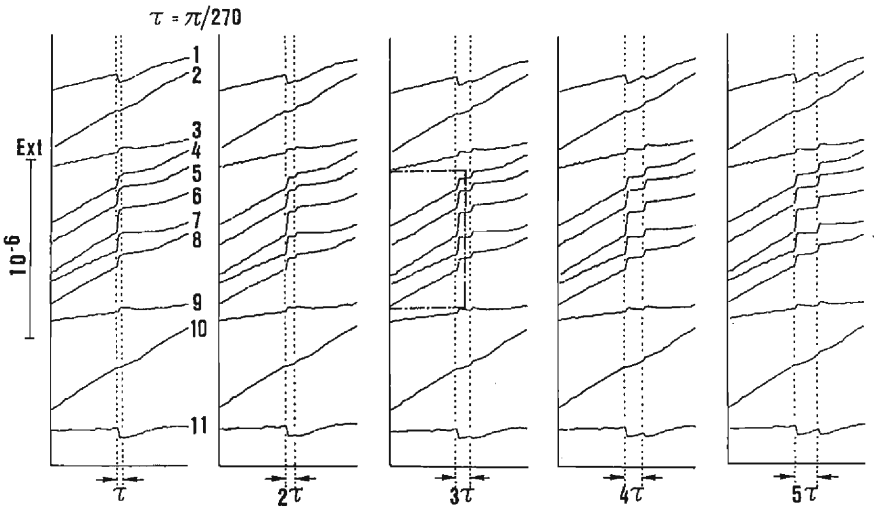

Fig. 18a. Strain variations originated by two successive earthquakes. The case that differential coefficients of strain variations are positive is shown. τ corresponds to 2/3 days in this simulation. The surrounded area in the middle of the figure is enlarged and shown in Fig. 18c.

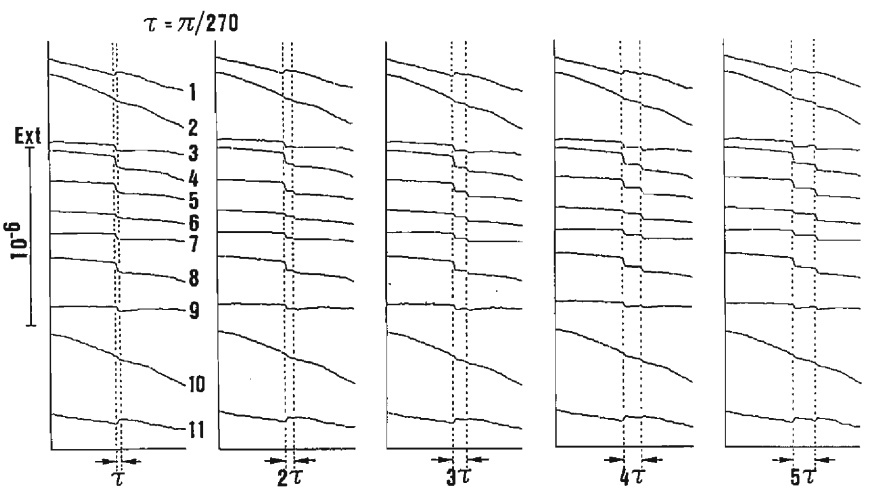

Fig. 18b. Strain variations in the case of negative differential coefficients.

(4) Strain steps are generally small when absolute values of differential coefficients of strain variations are small **(Fig. 17)**.

(5) As for two strain steps caused by two successive earthquakes, the step amplitudes by the latter earthquake are smaller than those of the former earthquake when the time interval between the two earthquakes is sufficiently small **(Fig. 18)**.

These simulated results coincide well with the characteristics of the observed strain

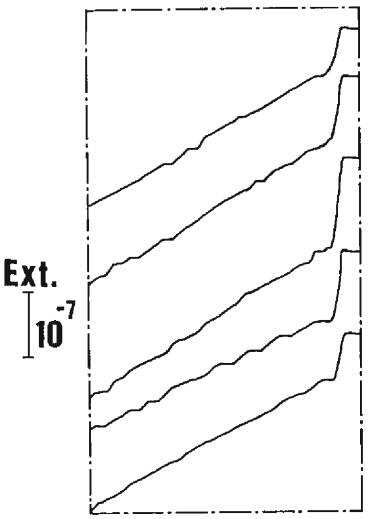

Fig. 18c. Examples of non-seismic strain steps. The surrounded area in **Fig. 18a** is enlarged to show non-seismic steps clearly.

steps mentioned in section 3.4. Therefore, it can be said that our mechanical model with a simulated structure around the observing site shows that surface temperature variations contribute to the strain energy.

7. Discussion

In the simulation by our mechanical model, it is assumed that the frictional coefficients decrease with seismic ground motions. The decrease of the frictional constants should range between some bounds. A number of tests have shown that a 90% decrease can reasonably well simulate the observations. The actual mechanism corresponding to this decrease is an important clue to understand the behavior of a fractured zone.

External forces such as tectonic stress or tidal forces are not concerned with the present analysis. Tectonic strain rate may be of the order of 10^{-7} strain/year or so, and tidal strains are of the order of 10^{-8} strain, while the amplitudes of annual strain variations caused by surface temperature reach to 5×10^{-6} strain in our case. Therefore, most strain variations in the Yasutomi Observation Vault may be induced by the surface temperature variations.

Nakahori (1977)[11] and Taniguchi and Oike (1984)[12] found large amplitudes of tidal strain variations and surface wave amplitudes at the fractured zone of the Yasutomi fault. On the contrary, in our simulations, low elastic coefficient portions showed small amplitudes of variations. This apparent discrepancy supports our model because our simulations concern only internal force such as thermal-deformation stress and not external forces such as tectonic and tidal stresses.

Strain steps which have no relation with seismic ground motions are sometimes recorded. Their amplitudes are, in general, smaller than 5×10^{-8} strain. It can be considered that such non-seismic strain steps are observed when locally accumulated strain exceeds some threshold level. **Fig. 18c** shows some examples of non-seismic strain steps. Those amplitudes, though small in the figure, are dependent on the frictional coefficients and are variable in the simulation. It is considered that these non-seismic strain steps also may reflect the frictional condition in and around the observation site.

As mentioned in section 2, traffic ground motions of the expressway just above are always remarkable. Nevertheless, strain steps are scarcely caused by those traffic ground motions. In general, traffic ground motion originating on the ground surface decreases rapidly both with depth and horizontal distance. That is to say, traffic ground motion concerns only a small area. In contrast, seismic wave length is so long in general that seismic waves transmit through whole of the fault zone without changes in their amplitudes. In order to release the locally accumulated strain, it may be necessary for the whole of the concerned area to vibrate. Therefore, the fractured zones which seem to control the amplitudes of strain steps are considered to exist widely in the basement rock.

In future, it is important to investigate how seismic ground motion decouples the various basement rock at interfaces, and how they originate strain steps. From our observational experiences, we can imagine that this process may relate to the transfer of crustal materials, such as soil gas and underground water. This process is also suggestive in investigating geoelectric, geomagnetic and geochemical phenomena as precursors of earthquakes.

8. Conclusions

The Yasutomi Observation Vault is situated inside the fault zone and its overburden depth is shallow. In this article, we analyzed the strain steps observed at the Yasutomi Observation Vault and revealed some of the characteristic behavior of the fractured zones. The results are as follows:

(1) In many cases, the previously accumulated strain around the observation site is released by coseismic strain steps. The amplitudes of observed strain steps are frequently larger than those theoretically expected.

(2) Seismic waves often trigger strain steps, releasing such locally accumulated strain.

(3) The polarities of strain steps of each component seem to distribute randomly in space. This may be caused by the heterogeneity of the physical properties of the basement rock.

(4) The pattern of strain release by strain steps depends on the fault strike. In the case of the Yasutomi fault, the strain changes in the direction normal to the fault zone is predominant for strain steps. The pattern of this thickness change of the fault zone derived from strain steps corresponds to that observed for long-term strain variations.

(5) Non-seismic strain steps are occasionally observed and some amount of locally accumulated strain is released by those steps.

(6) The energy source of the locally accumulated strain is thermal deformation caused by the annual variations of surface temperature.

Acknowledgments

The author wishes to express his sincere thanks to Y. Kishimoto for encouragement throughout this study and critical reading of the manuscript. The author would like to thank K. Oike, T. Tanaka, T. Mikumo and N. Sumitomo for their valuable discussions, encouragement and critical reading of the manuscript. F. Takeuchi provided valuable discussions. R. Nishida and K. Nishigami kindly provided useful data. S. Matsuo assisted in the observations. The Tottori Microearthquake Observatory of Kyoto University, Japan Highway Public Corporation and Yasutomi Town kindly allowed us to quote valuable data and provided observation facilities. The appreciation of the author to all of the above is great.

References

1) Press, F.: Displacements, Strains, and Tilts at Teleseismic Distances, Jour. Geophys. Res., Vol. 70, No. 5, 1965, pp. 2395–2412.
2) Sato, R. and M. Matsu'ura: Strains and Tilts on the Surface of a Semi-infinite Medium, Jour. Phys. Earth, Vol. 22, 1974, pp. 213–221.
3) Matsu'ura, M. and R. Sato: Displacement Field due to the Fault, Jour. Seis. Soc. Japan, Vol. 28, 1975, pp. 429–434 (in Japanese).
4) Matsu'ura, M., T. Tanimoto and T. Iwasaki: Quasi-Static Displacement due to Faulting in a Layered Half-Space with an Intervenient Viscoelastic Layer, Jour. Phys. Earth, Vol. 29, 1981, pp. 23–54.
5) Wideman, C. J. and M. W. Major: Strain Steps Associated with Earthquakes, Bull. Seis. Soc. Amer., Vol. 57, No. 6, 1967, pp. 1429–1444.
6) Takemoto, S. and M. Takada: Study on Strain Steps Associated with Earthquakes, Jour. Geodetic Soc. Japan, Vol. 15, No. 2. 3, 1969, pp. 68–74 (in Japanese).
7) Oike, K., K. Watanabe, K. Nakamura, K. Taniguchi and Y. Kishimoto: On the System for the Continuous Observation in a Test-field for the Earthquake Prediction at the Yamasaki Fault, Annuals, Disas. Prev. Res. Inst., Kyoto Univ., No. 24B-1, 1981, pp. 29–40 (in Japanese).
8) Watanabe, K., K. Oike, K. Nakamura and Y. Kishimoto: On the Characteristics of Long-period Strain Change in the Yasutomi Observation Tunnel at the Yamasaki Fault, Annuals, Disas. Prev. Res. Inst., Kyoto univ., No. 26B-1, 1983, pp. 87–94 (in Japanese).
9) Watanabe, K.: Strain variations of the Yamasaki Fault Zone, Southwest Japan, Derived from Extensometer Observations, Part 1, —On the Long-term Strain Variations—, Bull. Disas. Prev. Res. Inst., Kyoto Univ., Vol. 41, No. 1 (in Press).
10) Electromagnetic Research Group for the Active Fault: Low Electrical Resistivity along an Active Fault, the Yamasaki Fault, Jour. Geomag. Geoelectr., Vol. 34, 1982, pp. 103–127.
11) Nakahori, Y.: On the Tidal Strain Observed in the Yasutomi Observation Tunnel at the Yamasaki Fault, Master Thesis, Kyoto Univ., 1977 (in Japanese).
12) Taniguchi, K. and K. Oike: Behavior of Fractured Zones at the Yamasaki Fault for Teleseismic Surface Waves, Jour. Phys. Earth, Vol. 32, 1984, pp. 449–461.
13) Taniguchi, K. and K. Oike: Behavior of Fractured Zones at the Yamasaki Fault for S Wave, Annuals, Disas. Prev. Res. Inst., Kyoto Univ., No. 29B-1, 1986, pp. 49–58 (in Japanese).
14) Japan Highway Public Corporation: Personal Communication.
15) Nishigami, K.: Personal Communication.

16) Nishida, R.: Jishin no Hasshinkikou, The Earth Monthly, Vol. 7, No. 1, 1985, pp. 49–53 (in Japanese).
17) Tottori Microearthquake Observatory: Personal communication.
18) Oike, K.: On a List of Hypocenters Compiled by the Tottori Microearthquake Observatory, Jour. Seis. Soc. Japan, Vol. 28, 1975, pp. 331–346, (in Japanese).
19) Utsu, T. (Edit): Zishin no Jiten, Asakura Shoten, 1987, pp. 243–244 (in Japanese).
20) Nishigami, K. and T. Tsukuda: Jishin no Hassei-katei, The Earth Monthly, Vol. 7, No. 1, pp. 43–49 (in Japanese).
21) Sawaragi, Y. and H. Tokumaru: On Fundamental Equation of The Dynamical Behaviors of Nonlinear Visco-Elastic Bodies, Memoirs of Fac. Eng., Kyoto Univ., Vol. 16, 1954, pp. 100–111.
22) Kasahara, K.: A Simulation of Energy Release Process in a Seismic Region, Proc. Japan Acad. Vol. 43, 1967, pp. 483–488.
23) Otsuka, M.: A Simulation of Earthquake Occurrence, Part 1. A Mechanical Model, Jour. Seis. Soc. Japan, Vol. 24, 1971, pp. 13–25 (in Japanese).
24) Knopoff, L., J. O. Mouton and R. Burridge: The Dynamics of a one-dimensional Fault in the Presence of Friction, Geophys. J. R. astr. Soc., Vol. 35, 1973, pp. 169–184.
25) Nur, A.: Nonuniform Friction as a Physical Basis for Earthquake Mechanics, Pageoph, Vol. 116, 1978, pp. 964–989.